Measuring elastic properties of cells by evaluation of scanning acoustic microscopy $V(z)$ values using simplex algorithm

T. Kundu,* J. Bereiter-Hahn,‡ and K. Hillmann‡

*Department of Civil Engineering and Engineering Mechanics, University of Arizona, Tucson, Arizona 85721 USA; and ‡Cinematic Cell Research Group, Johann Wolfgang Goethe University, D-6000 Frankfurt am Main, Federal Republic of Germany

ABSTRACT In this paper a new technique is proposed to determine the acoustic properties as well as the thickness (and volume) of biological cells. Variations of thickness, density, acoustic wave velocity, stiffness, and attenuation coefficient of a living or dead cell are obtained by scanning the cell by an acoustic microscope. The distance between the cell and the microscope lens is varied and several voltage curves are thus obtained. These curves are then inverted by simplex optimization technique to obtain the cell parameters. The spatial resolution of the method is limited to the resolution of the scanning acoustic microscope. It allows to take advantage of the full range of frequencies and amplification of the microscope. Characteristic distributions of stiffness are exemplified with an endothelial cell in culture. The main part of the thin, lamellar cytoplasm has high stiffness, which drops close to the lamella/cell body transition region and only slightly increases again through the central part of the cell. Acoustic attenuation seems to be related to two factors, cytoplasm accumulation (in the lamellar parts) and scattering in the central part rich in organelles.

INTRODUCTION

The mechanical properties of cells are not well understood. There are good reasons to assume physiological significance in differentiation, metabolic control, and interaction of cells with their environment (Bereiter-Hahn, 1987*c*, 1988; Elson, 1988; Levesque et al., 1989). This is obvious for blood cells which are deformed while passing through or traversing capillaries (Worthen et al., 1989; Waugh and Hochmuth, 1987), and it also applies to bone and muscle cells. Cytoplasm is best modeled as a viscoelastic body resisting strain by elastic stiffness and exhibiting relaxation on being deformed. Thus the speed and frequency of force application are determinants for the value obtained for elastic stiffness. Pure elasticity measurements are possible only at relatively fast and low amplitude force applications.

Acoustic microscopy in principle allows to distinguish between modulation of the signal by the viscous properties of a material and its elastic properties. The first is represented by acoustic attenuation, the latter by impedance (density multiplied by the acoustic wave velocity). Deformation by the ultrasound waves is extremely small (in the subnanometer range), and frequency is very high (1–2 GHz). Thus acoustic microscopy is a unique tool for the investigation of mechanical properties of cells. However, the methods of analysis of viscoelastic bodies are still in their infancy.

Address correspondence to Prof. Dr. J. Bereiter-Hahn, Cinematic Cell Research Group, Johann Wolfgang Goethe University, P.O.B. 11 19 32, D 6000 Frankfurt/M, FRG.

In the last decade several efforts have been made to obtain elastic properties of a variety of materials by the acoustic microscopy technique. This is done by analyzing the $V(z)$ curve which is also known as the acoustic material signature (AMS) of the investigated specimen. $V(z)$ curves show the variation of voltage generated by an acoustic microscope as the distance between the microscope lens and the specimen varies. Different researchers used $V(z)$ curves for measuring different properties of materials; Kushibiki et al. (1982*a*, 1983) evaluated velocity and attenuation of surface waves analysing the $V(z)$ curves, Weglein (1980, 1982) measured coating thickness; Kushibiki et al. (1982*b*) suggested the possibility of using it for material anisotropy investigation, Briggs and his associates (Daft et al., 1985) used it for crack detections, Yamanaka et al. (1982) measured rates of surface hardening, Kino and his associates (Liang et al., 1982) measured residual stress patterns in materials, Hildebrand and Rugar (1984), Litniewski and Bereiter-Hahn (1990) determined elastic properties of living and dead cells from $V(z)$ analyses. Every investigator computed $V(z)$ curve with different simplifying assumptions which are appropriate for analysis. Then experimental $V(z)$ were properly compared with theoretical $V(z)$ to obtain parameters of interest.

The simplex optimization technique (Nelder and Mead, 1965) is applied to the acoustic microscopy analysis to obtain thickness, density, acoustic wave velocity, and attenuation coefficient of living or dead cells. Investigations of biological cells by acoustic mi-

0006-3495/91/05/1194/14 $2.00

croscopy have been performed among others by Johnson et al. (1979), Hildebrand et al. (1981, 1982), Hildebrand and Rugar (1984), Bereiter-Hahn (1987*a*, 1987*b*), and Litniewski and Bereiter-Hahn (1990). Some of these investigations outlined a qualitative connection between image contrast and cellular elastic properties (Johnston et al., 1979; Hildebrand et al., 1981, 1982; Bereiter-Hahn, 1987*a*) and some others (Hildebrand and Rugar, 1984; Litniewski and Bereiter-Hahn, 1990) tried to obtain quantitative measurements of the elastic properties of cells on a microscopic scale. However, some difficulties are faced by the investigators who try to obtain quantitative measurements of cells. One such difficulty is the cell thickness measurement. The cell thickness can be obtained from the interference pattern produced by rays reflected from the top of the cell (at the saline–cell interface) and from the bottom of the cell (at the cell–substrate interface). Because of this interference the cell is observed with a series of bright and dark rings in its acoustic image. These fringes are formed by constructive and destructive interferences due to the acoustical path difference between the two reflected rays, thus each ring identifies a region of constant cell thickness. A change of $\lambda/4$ in cell thickness produces 180° change in phase between the two reflected rays and hence a bright ring changes to a dark ring or vice-versa; λ is the longitudinal wave length of the acoustic wave in the cell. Thus, locations of the rings are correlated with the topography of the top surface of the cell, much as a topographic map describes the contour of a land surface. However, several difficulties are associated with the thickness measurements by counting such rings: first, the wavelength in the cell is not exactly known, one can at the most say that it is approximately equal to the wavelength in water. Thus it introduces some error. Secondly, the resolution (minimum measurement possible) of this technique is $\lambda/4$, so any change in thickness which is smaller than $\lambda/4$ cannot be detected by this technique. Thirdly, near the edge the cell thickness might be $< \lambda/4$ or the first observable dark ring near the edge can correspond to a thickness of $\lambda/4$ or any odd multiple of $\lambda/4$. Thus there is a high uncertainty in the edge thickness measurement. The difference in cell thickness between the edge and any point of interest can be estimated by counting rings between the edge ring and the ring passing through that point. So if there is an error in estimating the edge thickness then that error is introduced into all subsequent thickness measurements. In addition to the different sources of error mentioned above, it should be also kept in mind that since an increase as well as a decrease in cell thickness changes a dark ring to a bright one or vice-versa one cannot decide in which direction the cell thickness is increasing by only observing the ring pattern.

Thus there is more than one possible source of error in cell thickness measurements by the method using interference ring counting. An error in the thickness measurement would give rise to errors in the calculation of cell attenuation and cell impedance as well.

The method proposed in this paper avoids shortcomings of the presently available techniques, spatial resolution, and thickness measurements are not limited to the distances of interference maxima and minima. Temporal resolution, however, is decreased because several scans at different focus levels are required for the calculations.

2. THE CELL MODEL

The following considerations are based on the appearance of cells in culture. The cell and the substrate (e.g., a glass or a quartz coverslip) are modeled as a layered object similar to a previous study by Litniewski and Bereiter-Hahn (1990). The assumed layering is shown in Fig. 1. It consists of a liquid above the cell, a layer of cellular material and a semi-infinite substrate beneath the cell. The elastic properties of the liquid and the substrate are known while the elastic properties of the cell are to be evaluated. The basic assumption of this model is that the cell is flat over the extent of the acoustic beam. For simplicity, the model also assumes that the cell is closely adherent to the substrate, that the cellular material is homogeneous and that the acoustic microscope is measuring an average of the elastic

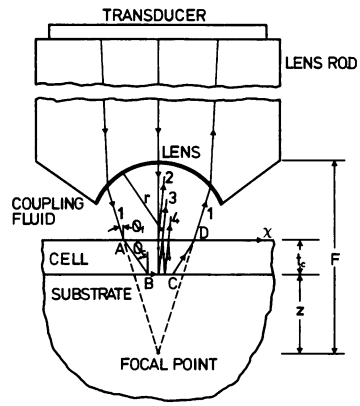

FIGURE 1 Schematic diagram of the experimental setup. Ray 1 is the critically reflected ray at Rayleigh angle, ray 2 is reflected from the top of the cell layer, ray 3 is reflected at the cell-substrate interface, ray 4 is reflected twice by the cell-substrate interface. Focal point shown in the figure is the point of focus in the saline in absence of the cell and substrate.

properties of this homogeneous region. Individual cell elements such as plasmamembrane, microfilaments, nucleus, etc. contribute to this average value. Whether a layer of culture medium between the cell and its substratum must be considered depends on the cell type and on the thickness of this space. The influence of such a layer is discussed in section 8. Relevant elastic properties for the model are given in Table 1. In this table P- and S-waves represent compressional (or primary) and shear (or secondary) waves. Both these two types of waves can propagate through a material which has nonzero shear modulus. However, only a P-wave can propagate through a liquid which has no shear strength. Acoustic waves are also P-waves because they produce only longitudinal (or normal) stresses and no shear stresses.

3. V(Z) COMPUTATION

The microscope lens is located above the cell as shown in Fig. 1. A coupling fluid (usually saline) connects the cell and the lens. It is now well known (Weglein, 1979; Parmon and Bertoni, 1979; Quate, 1980) that after being reflected by the object, principally two types of rays can reach the transducer, which is mounted at the top of the lens rod. One type of rays are critically reflected rays, generally at Rayleigh angles, ray 1 in Fig. 1. This ray undergoes some horizontal shift at the cell–substrate interface (Bertoni and Tamir, 1973). The second type are centrally reflected rays which strike the object vertically (rays 2, 3, and 4 in Fig. 1). Ray 2 comes back to the lens after being reflected by the top surface of the cell. Ray 3 reaches the transducer after being transmitted into the cell and reflected by the substrate. There are other rays (such as the ray 4 in Fig. 1) which go through multiple reflections inside the cell and then return to the lens. However, the intensities of these rays are small compared with other rays, hence one can neglect these third and higher order reflections.

In Fig. 1 the radius of curvature of the lens is denoted by r, F is the focal length of the lens, and z is the distance between the focal point and the cell–substrate interface. We assume z to be positive when the focal point is below the interface as shown in the figure. The focal length (F) and radius of curvature (r) are related in a complex manner (see Kundu, 1990), however for small α_f/α_s or small lens angle this relation is simplified to

$$F \approx r/(1 - \alpha_f/\alpha_s), \tag{1}$$

where α_f and α_s are acoustic wave velocities in the coupling fluid and the lens material, respectively.

TABLE 1 Mechanical properties of cells, coupling fluid, substrate, and lens material

Material	Density Γ	P-wave speed α	S-wave speed β	Attenuation coef. a
	gm/cc	*km/s*	*km/s*	$1/\mu m$
Saline/Water (Coupling fluid)	1.0	1.5	—	0.03
Glass (Substrate)	2.47	5.87	3.70	0.0
Cell	1.02–1.08	1.5–1.8	—	0.03–0.09
Sapphire (Lens material)	4.0	11.1	6.25	0.0

3.1 V(z) of cell on substrate

Let us first obtain the voltage generated by ray 2. The distance traveled by ray 2 in the coupling fluid is $2(F - z - t_c)$, where t_c is the thickness of the cell. So the phase change and the attenuation of the ray for traveling this path is given by $\exp\{2ik_f(F - z - t_c)\}$ and $\exp\{-2a_f(F - z - t_c)\}$, respectively, where a_f is the attenuation coefficient in the coupling fluid and $k_f(=\Omega/\alpha_f)$ is the compressional wave number in the coupling fluid, Ω is the circular frequency of the acoustic wave. To obtain the amplitude of the reflected beam, one needs to multiply the incident beam strength by the reflection coefficient $R(m_1, m_2, \Theta)$, where m_1 is medium 1 that contains the incident and reflected beams. The incident beam is reflected by medium 2 or m_2, and Θ is the angle of incidence. The expression of $R(m_1, m_2, \Theta)$ is given in the Appendix. So in our case, the reflection coefficient for ray 2 should have the form $R(f, c, 0)$, where f represents the coupling fluid, c stands for the cell, and the incident angle Θ is 0.

Since the incident beam is a converging beam its strength, and hence the reflected beam strength is a function of the distance between the focal point and the reflecting surface. If this distance is reduced, the beam strength increases. Finally, the voltage produced by ray 2 (V_2) is obtained by simply multiplying the propagation term, the attenuation term, the reflection coefficient, and a function $P(z + t_c)$ as given below.

$$V_2(z) = P(z + t_c) \cdot R(f, c, 0) \cdot \exp\{2ik_f(F - z - t_c) - 2a_f(F - z - t_c)\}. \tag{2}$$

The function $P(z + t_c)$ is introduced to incorporate the converging nature of the incident beam. Its unit is the same as $V(z)$. Other factors that affect the final voltage output, such as amplification and distortion of the signal inside the scanning acoustic microscope (ELSAM) electronic circuits, attenuation of signals during its travel through the lens rod, and coupling fluid are also included in the function $P(z + t_c)$. This function has to be obtained experimentally.

In the same manner one can compute the voltage produced by ray 3

$$V_3(z) = P(z) \cdot T(f, c, 0) \cdot R(c, g, 0) \cdot T(c, f, 0) \cdot \exp\{(2ik_f - 2a_f)(F - z - t_c) + 2ik_c t_c - 2a_c t_c\}, \quad (3)$$

where $T(f, c, 0)$ and $T(c, f, 0)$ are transmission coefficients for fluid to cell and cell to fluid transmissions, respectively, with incident angle equal to zero. General expression of $T(m_1, m_2, \Theta)$ is given in the Appendix. In the reflection coefficient $R(c, g, 0)$, g stands for the substrate; in our experiment glass substrate was taken. $k_c(=\Omega/\alpha_c)$ is the acoustic wave number and a_c is the attenuation coefficient of the cell.

Next the voltage produced by the critically reflected ray, ray 1 of Fig. 1, is to be obtained. For this purpose the path lengths traveled by this ray in different media are computed. The length of the path traveled by ray 1 in the coupling fluid is $2\{f - (z + t_c)\,\mathrm{s}\,\Theta_f\}$. The distance traveled inside the cell is $(2t_c \cdot \mathrm{s}\,\Theta_c)$ and at the glass–cell interface it is equal to $2\{(z + t_c)\tan\Theta_f - t_c \cdot \tan\Theta_c\}$. The critically incident beam generates Rayleigh surface waves at the cell–substrate interface, that causes the offset BC. The wave propagates as a Rayleigh surface wave between points B and C.

So the voltage produced by ray 1 is given by

$$V_1(z) = P(z) \cdot T(f, c, \Theta_f) \cdot R(c, g, \Theta_c) \cdot T(c, f, \Theta_c) \cdot \exp\{2(ik_f - a_f)[F - (z + t_c)\,\mathrm{s}\,\Theta_f] + 2t_c(ik_c - a_c)\,\mathrm{s}\,\Theta_c + 2(ik_r - a_r) \cdot [(z + t_c)\tan\Theta_f - t_c \tan\Theta_c]\}, \quad (4)$$

where a_r is the attenuation coefficient of the Rayleigh wave, as it travels from B to C, $k_r = \Omega/C_r$ and C_r is the Rayleigh wave velocity in the substrate. Critical angles Θ_f and Θ_c are functions of α_f, α_c, and C_r,

$$\Theta_f = \arcsin(\alpha_f/C_r)$$
$$\Theta_c = \arcsin(\alpha_c/C_r) \quad (5)$$

so,

$$k_r = k_f \cdot \sin\Theta_f = k_c \cdot \sin\Theta_c. \quad (6)$$

After substituting Eq. 6 into Eq. 4 one obtains after some algebraic manipulations

$$V_1(z) = P(z) \cdot T(f, c, \Theta_f) \cdot R(c, g, \Theta_c) \cdot T(c, f, \Theta_c) \cdot \exp\{2ik_f[F - (z + t_c)\cos\Theta_f] + 2ik_c t_c \cos\Theta_c - 2a_f[F - (z + t_c)\,\mathrm{s}\,\Theta_f] - 2a_c t_c\,\mathrm{s}\,\Theta_c - 2a_r[(z + t_c)\tan\Theta_f - t_c\tan\Theta_c]\}. \quad (7)$$

It should be noted here that $\exp\{2ik_f F - 2a_f F\}$ appears in the right-hand side of Eqs. 2, 3, and 7. If a new function $p(z)$ is defined such that

$$p(z) = P(z) \cdot \exp\{2ik_f F - 2a_f F\} \quad (8)$$

then V_1, V_2, and V_3 take the following form

$$V_1(z) = p(z) \cdot T(f, c, \Theta_f) \cdot R(c, g, \Theta_c) \cdot T(c, f, \Theta_c) \cdot \exp\{-2ik_f(z + t_c)\cos\Theta_f + 2ik_c t_c \cos\Theta_c + 2a_f(z + t_c)\,\mathrm{s}\,\Theta_f - 2a_c t_c\,\mathrm{s}\,\Theta_c - 2a_r[(z + t_c)\tan\Theta_f - t_c\tan\Theta_c]\}$$
$$V_2(z) = p(z + t_c) \cdot R(f, c, 0) \cdot \exp\{2(a_f - ik_f)(z + t_c)\}$$
$$V_3(z) = p(z) \cdot T(f, c, 0) \cdot R(c, g, 0) \cdot T(c, f, 0) \cdot \exp\{2(a_f - ik_f)(z + t_c) + 2t_c(ik_c - a_c)\}. \quad (9)$$

Now the total voltage is the sum of these three voltages

$$V_c(z) = V_1(z) + V_2(z) + V_3(z). \quad (10)$$

The subscript c indicates that this voltage is obtained over the cell. It should be mentioned here that if the critical angle Θ_f is greater than the half angle of the lens then $V_1(z) = 0$ and $V_c(z) = V_2(z) + V_3(z)$.

3.2 V(z) of substrate

$V(z)$ of the substrate in absence of the cell can be obtained in the same manner as before. However, in this case only two rays are to be considered, one critically reflected ray and one centrally reflected ray. The voltage generated by these two rays can be easily obtained by simply putting $t_c = 0$ in the expressions of V_1 and V_3 in Eq. 9 and omitting the transmission coefficients. Thus one gets

$$V_4(z) = p(z) \cdot R(c, g, \Theta_f) \cdot \exp\{-2ik_f z \cdot \cos\Theta_f + 2a_f z \cdot \sec\Theta_f - 2a_r)z \cdot \tan\Theta_f\}$$
$$V_5(z) = p(z) \cdot R(f, g, 0) \cdot \exp\{2z(a_f - ik_f)\} \quad (11)$$

and

$$V_g(z) = V_4(z) + V_5(z). \quad (12)$$

Subscript g stands for the glass substrate.

4. EXPERIMENTAL INVESTIGATION

For the experimental investigation a scanning acoustic microscope (ELSAM, Wild-Leitz, Wetzlar) operated at 1 GHz frequency has been used. The acoustic lens made of sapphire had a radius of curvature of 40 μm and an opening half-angle of 50°. Length of the lens rod (distance between the lens and the transducer) was

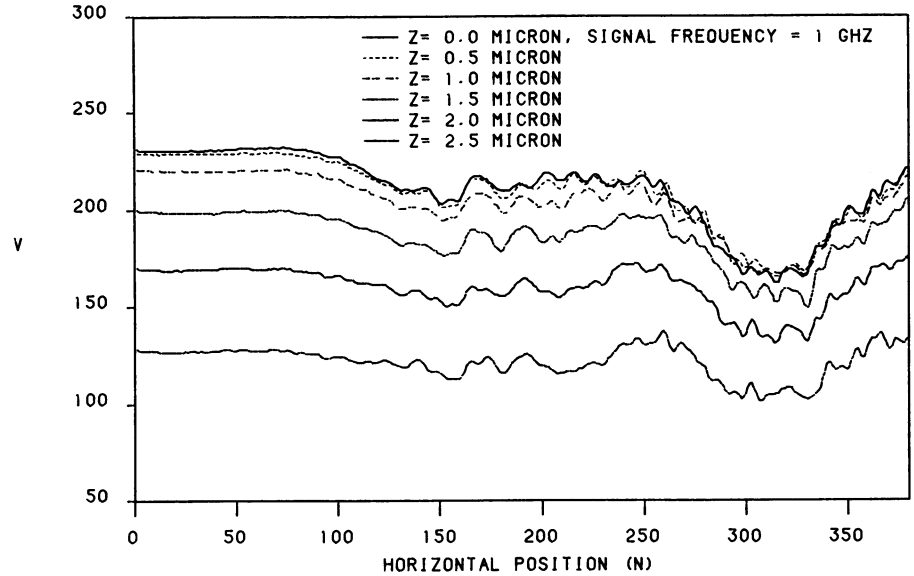

FIGURE 2 Scan lines through a living cell on glass at different z values.

2,000 μm and the transducer radius 50 μm. Acoustic properties of sapphire and the coupling fluid (saline) are given in Table 1.

The cell as well as the substrate is scanned horizontally by the acoustic lens for different values of z, starting from $z = 0$ up to $z = 2.0$ μm or more at an interval of 0.5 μm. Thus different scan lines $V(x)$ are obtained at different values of z. For calculation purposes the signal/noise ratio is increased by averaging 120 scans per line. An example of a set of scan lines is shown in Fig. 2. In this figure a total length of 78 μm is discretized into 380 points (pixels, N). So one unit in the horizontal position (N) along the abscissa of Fig. 2 represents a distance of 0.2 μm along the scan line. One can see from this figure that the received signal becomes more and more weak as z increases and for z greater than some critical value z_c (in this case $z_c \approx 3.8$ μm) it is almost equal to zero. One reason for it is that as z increases, defocussing increases, thus the incident and reflected signal strengths become gradually weaker. A second reason can be stated like this, for large z the reflected signal returns to the transducer before the time gate for receiving the signal is activated. Hence the transducer cannot sense any reflected signal for z greater than z_c. Whatever may be the reason $p(z)$ of Eqs. 9 and 11 should be able to show a trend similar to the observed $V_c(z)$ and should be equal to zero for z greater than z_c.

If we consider a specific value of N in Fig. 2, say $N = 5$ (or 200, or 300) and plot voltages against z, we get $V(z)$ plot for that N as shown in Fig. 3. The line without any marker corresponds to $N = 5$, the line with square markers is for $N = 200$ and the line with star markers is obtained at $N = 300$. Since the point $N = 5$ is located above the glass substrate this $V(z)$ plot should correspond to the $V(z)$ of glass, or $V_g(z)$ of Eq. 12. $V(z)$ at $N = 200$ and 300 correspond to $V_c(z)$ of Eq. 10 since these positions are above the cell.

5. ANALYSIS

From known acoustic properties of sapphire, water, and glass (see Table 1), $V_4(z)$ and $V_5(z)$ of Eq. 11 and hence

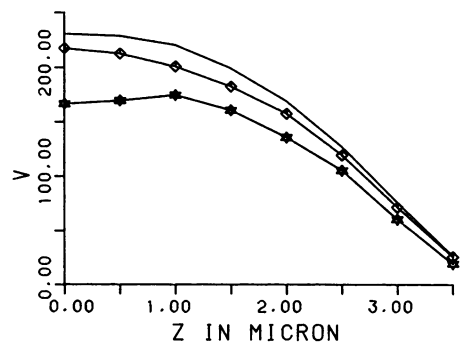

FIGURE 3 Experimental $V(z)$ at $N = 5$ (line without any marker), 200 (line with square markers), and 300 (line with star markers).

$V_g(z)$ can be computed in terms of the unknown functions $p(z)$. $p(z)$ is then assumed to be a second order polynomial of z, for z less than z_c,

$$p(z) = a + bz + cz^2, \quad \text{for } z < z_c$$
$$= 0, \quad \text{for } z > z_c. \tag{13}$$

The unknown coefficients a, b, and c are obtained by matching the computed $V_g(z)$ with the experimental values by the least squares error minimization technique. Since this technique is well known, the detail derivation is omitted here and only the final results are given.

$$(a, b, c)^T = [A]^{-1} \cdot (\Sigma g_i \cdot V_i,\ \Sigma g_i \cdot V_i \cdot z_i,\ \Sigma g_i \cdot V_i \cdot z_i^2)^T. \tag{14}$$

In the above equation the superscript T denotes the transpose of the row vectors, V_i is the experimentally obtained voltage at $z = z_i$, n is the number of z values for which the least squares matching is carried out, typically n is 4 or 5. $g_i = V_g(z_i)/p(z_i)$; so from Eq. 11,

$$g_i = R(f, g, \Theta_f) \cdot \exp\{-2ik_f \cdot z_i \cdot \cos\Theta_f + 2a_f \cdot z_i \cdot \sin\Theta - 2a_r \cdot z_i \cdot \tan\Theta_f\} + R(f, g, 0) \cdot \exp\{2z_i(a_f - ik_f)\} \tag{15}$$

and $[A]$ is a 3×3 matrix given by

$$[A] = \Sigma \begin{matrix} 1 & z_i & z_i^2 \\ z_i & z_i^2 & z_i^3 \\ z_i^2 & z_i^3 & z_i^4 \end{matrix} g_i^2 \tag{16}$$

After such matching at four points (z = 0, 0.5, 1.0, and 1.5 μm), Fig. 4 is obtained. In this figure the line without any marker represents the experimental $V_g(z)$ and the line with markers represents the computed $V_g(z)$. The two lines match very well up to z = 3.0 μm. A close matching at this stage is necessary to have confidence in subsequent analysis.

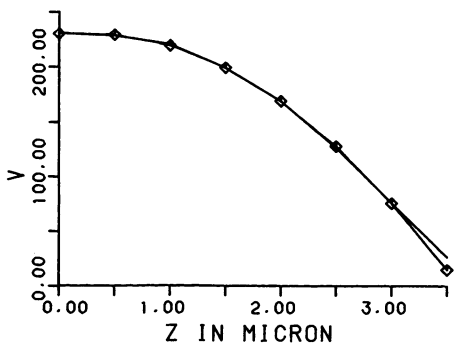

FIGURE 4 Experimental $V(z)$ (line without any marker) and computed $V(z)$ (line with markers) of glass at 1 GHz, both lines coincide very well, thus they can be distinguished only at $z > 3$ μm.

$V_c(z)$ for any assumed cell properties can be obtained from Eqs. 9 and 10 after $p(z)$ is known from the above analysis.

To check the reliability of the method, $V_c(z)$ is computed for two different layer (cell) thicknesses, 1 and 6 μm. Acoustic properties of the layer are assumed to have the following values, α_c = 1.6 km/s, density(Γ_c) = 1.04 gm/cc, a_c = 0.06. $V_c(z)$ thus computed are shown in Fig. 5. The line without any marker shows computed $V_g(z)$ of the glass substrate, the line with square markers is $V_c(z)$ of 1-μm thick layer and the line with star markers is $V_c(z)$ of 6-μm thick layer. It should be noted here that for a thin layer (t_c = 1 μm) $V_c(z)$ monotonically decreases, but for a thick layer (t_c = 6 μm) $V_c(z)$ first increases slightly then it starts to decrease. Experimental $V_c(z)$ also shows similar behavior (see Fig. 3). Thus the reliability of the method is verified in some qualitative sense. Next, some quantitative checking of the method is carried out. For this purpose it is investigated if α_c, Γ_c, a_c, and t_c can be correctly predicted from known values of $V_c(z)$ of Fig. 5. Simplex optimization technique is required for such back predictions of the layer parameters from its $V_c(z)$ curve.

6. SIMPLEX OPTIMIZATION TECHNIQUE

The purpose of the optimization is to determine a set of M parameters, in this case α_c, Γ_c, a_c, and t_c, which correspond to the smallest sum of the squares of the error, SQE, defined as

$$\text{SQE} = \Sigma\,(|V_c(z_i)| - V_i)^2, \tag{17}$$

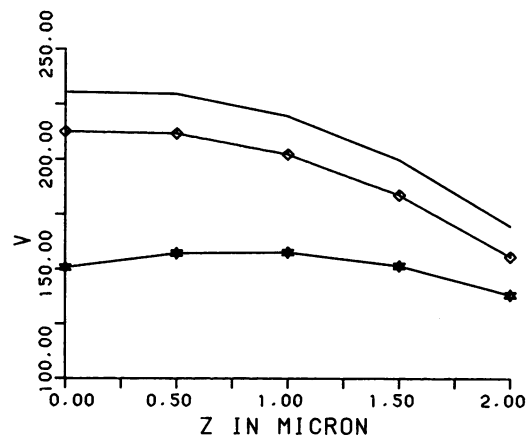

FIGURE 5 Computed $V(z)$ of glass (line without any marker), 1-μm thick cell (line with square marker), and 6-μm thick cell (line with star markers).

where m is the number of points $(z_1, z_2, \ldots, z_m)$ considered for optimizing M parameters. $|V_c(z_i)|$ is the amplitude of the computed voltage at z_i with some assumed set of parameters, and V_i is the given value of the voltage at z_i. For a unique solution, m should be greater than or at least equal to M.

The basic idea behind the simplex method (Nelder and Mead, 1965) is to consider each set of M variables as a point in a space of M dimensions. The point is called a vertex and a simplex is a geometrical figure which consists of $(M + 1)$ variables. If the total number of variables to be optimized is 2 ($M = 2$) then the simplex is a triangle ($M + 1 = 3$) in a two-dimensional space (Karim et al., 1990). The triangle ABW in Fig. 6 is such a simplex. The optimization starts by arbitrarily assigning some starting values to the $(M + 1)$ vertices. To obtain the lowest value of SQE, the simplex is moved according to the following rules: (*a*) find the vertices with the highest (worst) and lowest (best) SQE. (*b*) Replace the worst vertex by another vertex determined according to one of the four mechanisms: reflection, expansion, contraction, and shrinkage. (*c*) Continue the process until "satisfactory" values according to a certain predetermined criterion are obtained.

As an example, if a reflection is to be executed, the reflected vertex (R in Fig. 6) is created by extending a line from the worst vertex W through the center C of the remaining vertices (A and B in Fig. 6), so that the distance between R and C is equal to that between W and C. An expansion extends the reflected vertex by an amount equal to twice the distance between W and C (E in Fig. 6); a contraction moves the worst vertex half-way toward C (T in Fig. 6) and a shrinkage moves all vertices toward the best vertex (lowest E) by half their original distance from it. For a detailed discussion of the conditions for executing each of these four operations readers are referred to the paper by Nelder and Mead (1965).

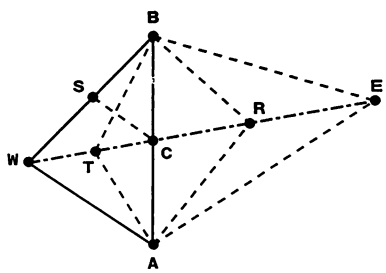

FIGURE 6 Two-dimensional simplex and its optimization mechanism. (After Karim et al., 1990.)

7. APPLICATION OF THE SIMPLEX METHOD

The method described in the previous section is now used to predict the layer parameters from a previously calculated $V(z)$ curve. Five points, shown by star markers in Fig. 5, are first considered for computing SQE of Eq. 17. Upper and lower bounds for each parameter are first decided. These bounds can be selected from some rough estimate of the parameter values. For example, an estimate of the thickness of the cell can be obtained from the past experience or by counting interference rings as described in section 1. For each parameter two upper bounds and two lower bounds are selected. One of these bounds can be identified as "absolute bounds," parameters must lie within these bounds. The second type of bounds can be called "probable bounds." Parameter values most probably lie within "probable bounds" but one is not absolutely sure about it. Meanings of these two types of bounds can be further clarified by considering the following example. Let us assume that the thickness of a cell is estimated to be 6.2 μm from the interference ring count. Considering different uncertainties in estimating the thickness by this technique one may say that most probably the thickness is between 5.5 and 7.0 μm, then these two bounds can be called "probable bounds." Now taking into account all possible sources of error if one can say with certainty that the thickness cannot be <5 μm and >8 μm, then these two values are "absolute bounds." Both these bounds are given as input to the simplex algorithm. "Probable bounds" are used to construct the initial simplex geometry and "absolute bounds" are needed to limit the region of search.

Initial simplex is constructed with five (=1 + number of unknown parameters) vertices. Coordinates of four vertices are obtained by taking "probable" upper bounds of three parameters and "probable" lower bound of the fourth parameter. "Probable" lower bounds of all four parameters are assigned as the coordinates of the fifth vertex. After going through a number of numerical exercises this type of initial simplex construction has been found to be most effective. Starting with this initial geometry, the simplex algorithm performs one or more of the four operations mentioned in section 6 and then gets rid of the worst vertex and includes a better vertex in the geometry after every iteration. Three combinations of upper and lower bounds are considered. Every combination generates a new initial simplex and defines a new region of search. These bounds for the four parameters are shown in Table 2. After 50 iterations,

TABLE 2 **Upper and lower bounds and computed layer parameters**

		Simplex 1	Simplex 2	Simplex 3
Bounds on α_c	Absolute	1.5–1.8	1.5–1.8	1.5–1.8
	Probable	1.55–1.7	1.55–1.7	1.55–1.7
Bounds on Γ_c	Absolute	1.01–1.1	1.01–1.1	1.03–1.05
	Probable	1.03–1.07	1.03–1.07	1.035–1.045
Bounds on a_c	Absolute	0.03–0.09	0.03–0.09	0.03–0.09
	Probable	0.04–0.07	0.04–0.07	0.04–0.08
Bounds on t_c	Absolute	5.0–8.0	5.8–6.5	5.0–8.0
	Probable	5.5–7.0	5.9–6.2	5.5–7.0
Converged values after 50 iterations	α_c (*km/s*)	1.602	1.600	1.600
	Γ_c (*gm/cc*)	1.055	1.060	1.044
	a_c (1/μm)	0.0604	0.0596	0.0598
	t_c (μm)	5.866	6.018	6.025

different initial simplex geometries converge to one set of values of α_c, Γ_c, a_c, and t_c. These values are also shown in Table 2.

Fig. 7 shows the parameter values as a function of the iteration number of trial number in the simplex algorithm. Three lines in every graph correspond to the three initial simplex geometries of Table 2. The line without any marker is for simplex 1, the line with star markers is obtained from simplex 2 and the line with square markers is generated by simplex 3. It can be seen from this figure and Table 2 that α_c (1.6) and a_c (0.06) converge very well for all three cases. Thickness t_c (6.0) shows a maximum error of 2.23% for simplex 1; however, when bounds on t_c are refined, in simplex 2, this error diminishes. Alternately, if bounds on density are refined keeping bounds on thickness unchanged (simplex 3) then also the error in t_c becomes negligibly small. Unlike the other three parameters, Γ_c (1.04) converges to three different values for three cases. So Γ_c predicted by this method is not very reliable. Fortunately, the cell density is approximately known, it is close to water but slightly higher. So an estimate of Γ_c between 1.02 and 1.08 gm/cc is reasonable. Hence, uncertainty in density comes only in the second decimal place. Previous studies (Litniewski and Bereiter-Hahn, 1990) showed that a_c/a_f is between 1 and 3, where $a_f(=0.03)$ is the attenuation coefficient of water, so "absolute bounds" of a_c should be 0.03 and 0.09. "Absolute" bounds of α_c are obtained similarly from previous studies, they are 1.5 and 1.8 km/s.

Simplex algorithm applied to the $V_c(z)$ of 1-μm thick layer also produced results with a similar order of error. Thus this quantitative check further confirms the reliability of the method.

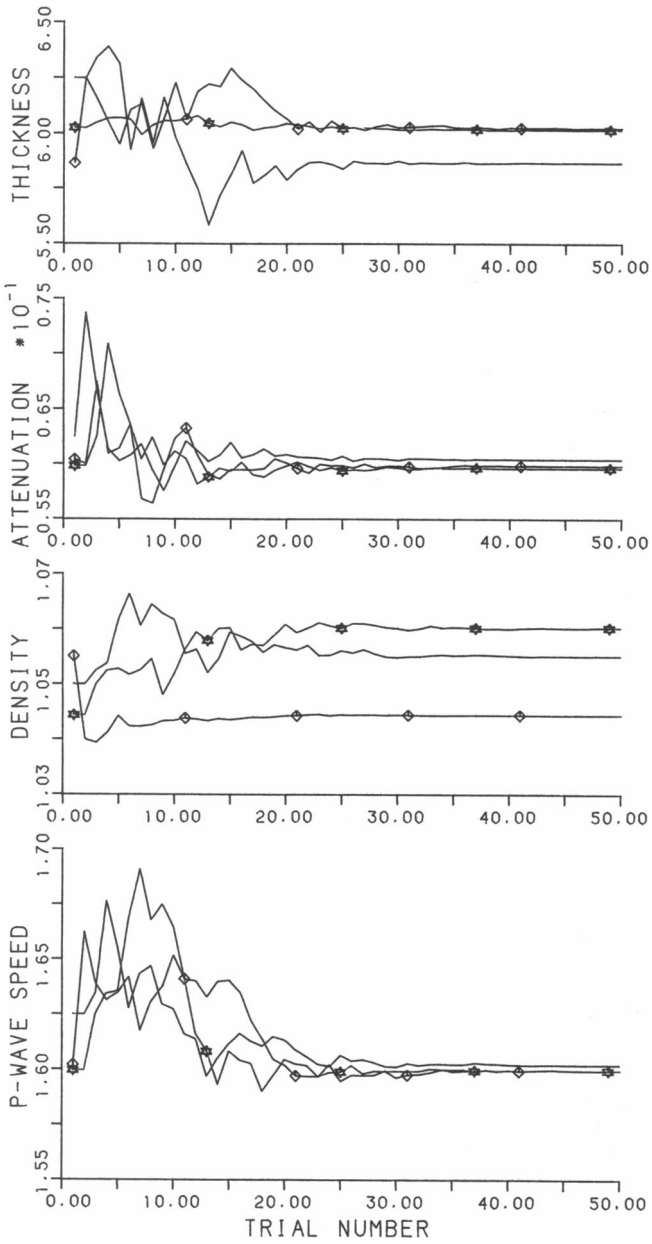

FIGURE 7 Different cell (layer) parameters as a function of the trial number in the simplex algorithm. Converged values are given in Table 2.

8. EFFECT OF THE COUPLING FLUID BETWEEN CELL AND SUBSTRATE

Up to this point of the analysis it has been always assumed that there is no gap between the cell and the substrate. However, in reality most cells are closely attached to the substrate at some regions only, whereas in the remaining area a thin layer of the coupling fluid

(generally saline or culture media) may be present between the cell and the substrate. The thickness of this liquid layer varies from the order of 0.02 μm to the order of 0.1 or 1 μm often reached near the central region of the cell (Izzard, 1976; Bereiter-Hahn et al., 1979). To understand the effect of this thin liquid layer on the $V(z)$ curve and on the cell parameter computation the cell model is extended by including a liquid layer between the cell and the substrate.

In this case calculations of four voltages (V_1, V_2, V_3, and V_4) generated by four rays are required. The critically reflected ray produces V_1, the central rays reflected from the top and bottom surfaces of the cell produces V_2 and V_3, respectively, and the central ray reflected by the substrate produces V_4. Higher order reflections are again neglected here. If t_f denotes the thickness of the coupling fluid between the cell and the substrate, then following similar steps as in section 3, these four voltage expressions can be obtained,

$$\begin{aligned}
V_1(z) &= p(z)\, T^2(f, c, \Theta_f)\, T^2(c, f, \Theta_c)\, R(f, g, \Theta_f) \\
&\quad \exp\{-2ik_f(z + t_c)\cos\Theta_f + 2ik_c t_c \cos\Theta_c \\
&\quad + 2a_f(z + t_c)\,\mathrm{s}\,\Theta_f - 2a_c t_c\,\mathrm{s}\,\Theta_c \\
&\quad - 2a_r[(z + t_c)\tan\Theta_f - t_c \tan\Theta_c]\} \\
V_2(z) &= p(z + t_c + t_f)\, R(f, c, 0) \\
&\quad \exp\{2(a_f - ik_f)(z + t_c + t_f)\} \\
V_3(z) &= p(z + t_f)\, T(f, c, 0)\, R(c, f, 0)\, T(c, f, 0) \\
&\quad \exp\{2(a_f - ik_f)(z + t_c + t_f) + 2t_c(ik_c - a_c)\} \\
V_4(z) &= p(z)\, T^2(f, c, 0)\, R(f, g, 0)\, T^2(c, f, 0) \\
&\quad \exp\{2(a_f - ik_f)(z + t_c) + 2t_c(ik_c - a_c) \qquad (18)
\end{aligned}$$

and the total voltage is the sum of these four voltages.

Two sets of $V(z)$ curves calculated for two (cell) layers of thicknesses 6 and 1 μm, respectively, with $\alpha = 1.6$ km/s, $\Gamma = 1.04$ gm/cc, and $a/a_f = 2$ are shown in Fig. 8. For each layer thickness $V(z)$ plots are given either without a second layer of fluid between the supporting glass and the layer under consideration or with second layers of different thicknesses.

Then the $V(z)$ values computed (considering the liquid layer between the cell and the substrate) are used in the simplex method as was done in section 7. It should be noted here that when the simplex algorithm is followed to predict the cell properties it is assumed that there is no liquid between the cell and the substrate similar to section 7. So this computation gives an estimate of the error introduced in the results for neglecting the liquid layer in our analysis.

Converged values of the layer parameters for the 6-μm thick layer with different liquid layer thicknesses can be seen in Fig. 9 and also in Table 3. Absolute and

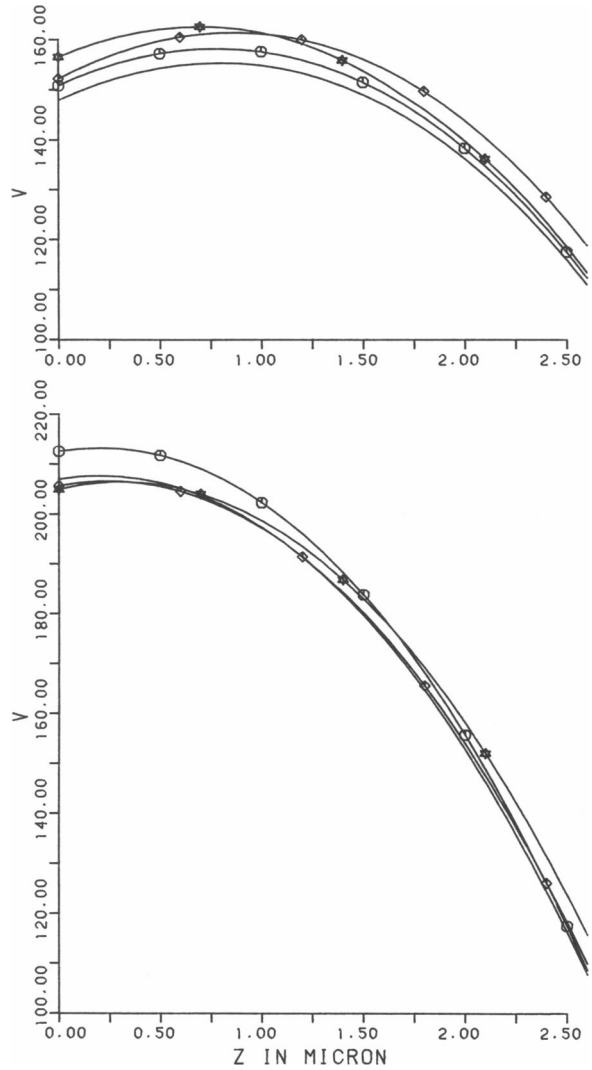

FIGURE 8 Computed $V(z)$ of 6-μm (*top*) and 1-μm (*bottom*) thick cell layer for different thicknesses of liquid layer between the cell and the substrate. In the top figure the line without any marker is for a 0.02-μm thick (t_f) liquid layer, lines with square and star markers correspond to $t_f = 0.2$ and 2.0 μm, respectively. In the bottom figure lines with no marker, with square and star markers correspond to $t_f = 0.03$, 0.06, and 0.12 μm, respectively. $V(z)$ of cells without any liquid layer are shown by the lines with circular markers.

probable bounds for Fig. 9 are identical to the simplex 1 of Table 2.

Similar convergence study is carried out for the 1-μm thick layer with different t_f values. For these computations absolute/probable bounds on α_c, Γ_c, a_c, and t_c are taken as 1.5–1.8/1.55–1.65, 1.02–1.08/1.03–1.05, 0.03–0.09/0.04–0.08, and 0.8–1.2/0.9–1.1, respectively. Converged values are tabulated in Table 3.

It can be seen from Table 3 that for 1 GHz signal frequency and 6-μm thick layer the maximum error in α_c

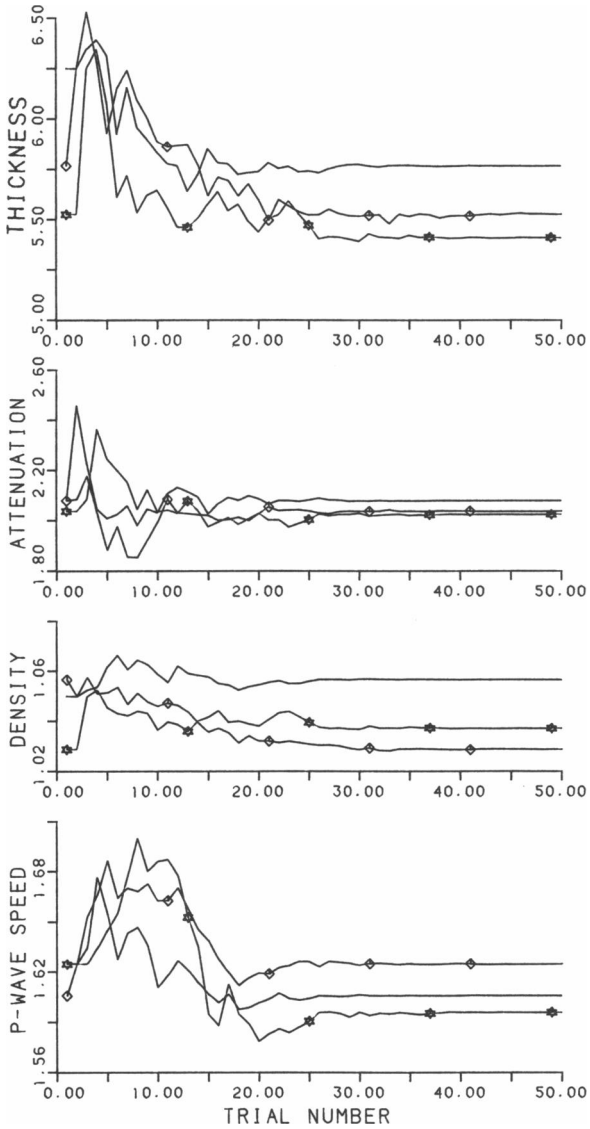

FIGURE 9 Different cell parameters for the 6-μm thick cell layer as a function of the trial number in the simplex algorithm. Three curves in each plot correspond to three values of t_f, 0.02 μm (lines without any marker), 0.2 μm (lines with square markers), and 2.0 μm (lines with star markers). Attenuation coefficient has been normalized with respect to that of water.

is only 1.56% at t_f = 0.2 μm. However, if one is interested in studying the difference between α_c and α_f ($\delta_\alpha = \alpha_c - \alpha_f$) instead of α_c then this small error magnifies significantly. 1.56% error on α_c is equivalent to 25% error on δ_α. Then this error is no longer negligible. Error in the attenuation is never more than 4% and for the thickness computation the maximum error is 10% for t_f = 2 μm.

For a 1-μm thick layer and 1 GHz signal frequency error in α_c increases from 0.75% to 7.88% as t_f increases

TABLE 3 **Computed cell parameters for different t_c, t_f, and signal frequencies**

Cell thickness/ signal frequency t_c/f	Liquid thickness between cell & glass t_f	Converged values after 50 trials α_c	Γ_c	a_c	t_c
μm/GHz	*μm*	*km/s*	*gm/cc*	*1/μm*	*μm*
6.0/1.0	0.02	1.606	1.057	0.0624	5.767
	0.20	1.625	1.029	0.0611	5.526
	2.00	1.596	1.037	0.0607	5.409
1.0/1.0	0.02	1.612	1.043	0.0620	1.057
	0.03	1.617	1.043	0.0603	1.075
	0.04	1.664	1.050	0.0571	1.093
	0.05	1.693	1.040	0.0638	1.073
	0.06	1.726	1.047	0.0609	1.094
1.0/1.5	0.02	1.597	1.035	0.0623	0.985
	0.03	1.595	1.028	0.0607	0.965
	0.04	1.594	1.035	0.0610	0.979
	0.05	1.610	1.033	0.0631	1.034
	0.06	1.612	1.042	0.0625	1.047
	0.12	1.575	1.031	0.0555	0.997

from 0.02 to 0.06 μm. Equivalent error on $\delta\alpha$ then varies from 12% (t_f = 0.02 μm) to 126% (t_f = 0.06 μm). Errors on attenuation (maximum is 6.33% for t_f = 0.05 μm) and thickness (maximum is 9.3% for t_f = 0.04 μm) are not significant.

The signal frequency can be increased to reduce the error on $\delta\alpha$. At 1.5 GHz frequency and for 1-μm thick layer (see Table 3) errors on α_c varies from 0.19% (t_f = 0.02 μm) to 1.56% (t_f = 0.12 μm); equivalent errors on $\delta\alpha$ then varies from 3% to 25%.

From these error studies one can see that for thin liquid layers ($<$0.03 μm for 1-μm thick cell and $<$0.2 μm for 6-μm thick cell), the analysis can be carried out neglecting the liquid layer. This simplified analysis only introduces a small error as long as the liquid layer is thin. If signal frequency is increased the error can be further reduced and then a relatively thicker liquid layer can be neglected during the analysis.

9. SIMPLEX ALGORITHM APPLIED TO THE EXPERIMENTAL DATA

Steps stated in section 7 are repeated here, but in this case, instead of computed $V_c(z)$ (markers in Fig. 5) we take experimental $V_c(z)$ (such as markers in Fig. 3) as V_1 of Eq. 17. Experimental $V_c(z)$ at different positions in the cell are obtained from Fig. 2. Five values of z (0, 0.5, 1, 1.5, and 2 μm) are considered for every horizontal position. Then simplex method is applied to every $V_c(z)$ to obtain the cell parameters at that position. Lower and

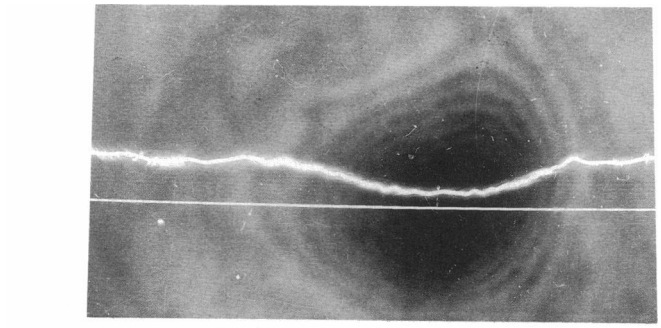

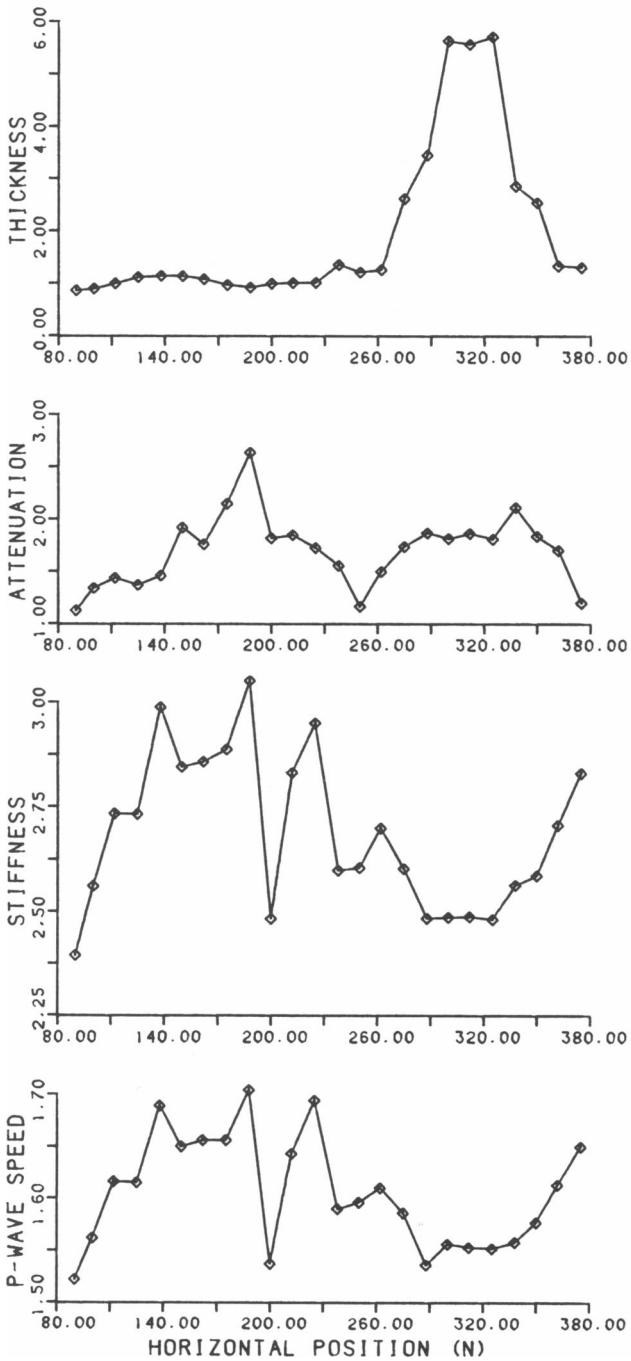

TABLE 4 Bounds on cell thickness at different points of the cell shown in Fig. 10

N	Absolute bounds	Probable bounds
	μm	μm
90–162	0.5–2.0	0.8–1.2
175–262, 362–375	0.5–2.0	1.0–1.5
275, 350	1.2–4.5	2.0–4.0
288, 338	2.5–5.5	3.0–4.0
300–325	4.0–8.5	5.0–7.0

upper bounds (absolute/probable) on α_c, Γ_c, and a_c are taken as (1.5–1.8/1.55–1.7), (1.02–1.08/1.03–1.05), and (0.03–0.09/0.04–0.08), respectively. Thickness of the cell is estimated by counting interference rings in the acoustic image of the cell, shown in Fig. 10. So bounds on the cell thickness depend on the position of the point of interest. Cell parameters are computed at 24 discrete N values, $N = 90, 100, 112, 125, 138, 150, 162, 175, 188, 200, 212, \ldots, 375$. Bounds on cell thickness for these N values are shown in Table 4.

Elastic stiffness or Young's modulus (Y) of any isotropic and linear elastic material can be expressed in terms of the acoustic wave velocity (α), Poisson's ratio (μ), and density (Γ) in the following manner

$$Y = g(\mu)\Gamma\alpha^2, \tag{19}$$

where

$$g(\mu) = [(1 + \mu)(1 - 2\mu)/(1 - \mu)]^2. \tag{20}$$

If Poisson's ratio of the cell is assumed to be independent of the horizontal position then $g(\mu)$ is constant in the cell. Hence, Young's modulus of the cell Y_c is proportional to E_c, where $E_c = \Gamma_c \cdot \alpha_c^2$. So a plot of E_c essentially shows the variation of elastic stiffness in the cell. Because of the unknown Poisson ratio no direct comparison of the values obtained by acoustic microscopy with the elasticity values derived from aspiration or poking experiments is possible. Regarding the dependence of elasticity on the strain rate (see e.g., Bereiter-Hahn, 1987*c*) one can assume an extremely high strain rate together with an extremely small deformation. Thus, impedance values reflect only elastic stiffness or Young's modulus, the viscous properties of cytoplasm are reflected by the attenuation of ultrasound, which, in addition, depends on scattering.

Fig. 10 illustrates the variations of t_c, a_c/a_f, E_c, and α_c

FIGURE 10 Acoustic image of a living XTH-2 cell on glass (*top*) and computed cell properties, thickness (t_c; μm), normalized attenuation (a_c/a_f), stiffness (E_c; GPa), (refer to Eq. 18, E_c is proportional to the Young's modulus but they are not exactly equal), and P-wave speed (α_c; km/s). The white straight line in the acoustic image is the scan line, the line above represents a single scan.

(from top to bottom) of a living endothelial cell on glass (XTH-2 cell). It should be noted here that E_c and α_c show similar type of variation. Because the density does not change significantly (it varies only in the second decimal place) E_c is essentially proportional to α_c^2.

The thickness of the thin cytoplasmic layer does not increase monotonically from the periphery to the central region, the accuracy of thickness calculations is sufficient to determine these very thin cytoplasmic areas.

The acoustic impedance (density multiplied by the P-wave velocity) and thus the elastic stiffness of the cell varies considerably with regions which are different in the organization of their cytoskeletal components. The pattern is similar to that described using a different method of analysis (Litniewski and Bereiter-Hahn, 1990). The actin fibrillar system can be assumed to represent the main determinant for acoustic properties (Bereiter-Hahn, 1987*a*, *b*; Worthen et al., 1989). In the cell shown in Fig. 10 at the very periphery (the region of the lamellipodium containing a diffuse meshwork of actin fibrils) elastic stiffness is low, steeply increasing toward the cell center. Along the main part of the thin lamellar cytoplasm elasticity remains relatively constant close to the margin of the dome-shaped cell center (starting at pixel 260). The central part of the cell ("cell body") is of low acoustic impedance. The lower values at pixels 200 and 230 to 240 coincide with a local swelling which can be seen in the thickness diagram and which is indicated in the acoustical image by a broadening of the interference fringe at this site. These observations coincide with observations on lymphocytes using the pipette method (Schmid-Schönbein et al., 1981). In these cells also the pseudopodia exhibited higher stiffness than the cell body.

Acoustic attenuation also varies along the scan line. In the very peripheral parts of the lamella (on the left side of the cell) with centripetally increasing impedance (pixels 78–140) attenuation is low and more or less constant while it increases steadily toward the center in the region of high impedance (pixel 140 to 180). A preliminary interpretation of this phenomenon is that it is related to a constant centripetal flow of the cortical actomyosin meshwork. This network is under tension (represented by the high impedance. Bereiter-Hahn, 1987*a* by continuous contraction toward the cell center accumulating material close to the margin of the dome-shaped cell body. The enhanced attenuation is supposed to result from accumulation of fibrillar material. We have shown in a previous study that specific attenuation (increase of attenuation per unit mass of protein) is much higher in the lamellar cytoplasm than in the central cytoplasm (Bereiter-Hahn et al., 1989). Due to the small density difference between water and protein, such a protein accumulation changes overall density only slightly although attenuation becomes more prominent. In the cell center attenuation again is rised to a medium level. This is due to a wealth of organelles responsible for scattering.

Assuming constant Poisson's ratio μ, elasticity changes by about a factor of 10. If we understand a cell being a hydraulic system, in equilibrium conditions the same pressure should be at any site of a cell counteracted by a corresponding tension at the cell surface. Local change of this tension at the surface should be followed by local swelling or shrinking, the speed of these processes being limited by the viscosity of cytoplasm resisting immediate flow. The low impedance values at pixels 200 and 230–240 are thought to represent such local weakenings. The difference in elastic stiffness between the center of the cell body and the lamella cytoplasm corresponds well with the ratio of the radii of curvature: assuming a spherical cell (radius R) with an internal pressure (P) which is balanced by the surface stress or membrane stress (T), their relation is described by

$$2T/R = P/t,$$

where t is the thickness of the membrane.

If we consider a cell being composed of interconnected spheres, the cell body with a radius R_c and the lamella area with radius R_l and the related tensions T_c and T_l at the surface, the pressure in a hydraulic system would be the same in both areas, therefore applies

$$T_c/T_l = R_c/R_l.$$

In the example shown in Fig. 8 the radius of curvature in the cell body area is ~ 43 μm, in the lamella area between pixel 90 and 190 the radius of curvature was estimated to be 500 μm. This ratio may explain the large differences in elasticity along the scan line in Fig. 10.

10. CONCLUDING REMARKS

The main assumption of this analysis is that the top surface of the cell is smooth and almost parallel to the substrate. Clearly when the angle between the top surface and the substrate is large ($>15°$ or 20°) (Litniewski and Bereiter-Hahn, 1990) then the results obtained by this analysis are not very reliable. However, well-spread cells in culture in general do not exceed this angle, thus they are well suited to be investigated by SAM.

This method gives good results if the initial estimates of the investigated parameters are reasonably good. If those estimates are quite far from the true values then the cell parameters may converge to a wrong set of values. So special attention should be given while

selecting the "absolute" and "probable" bounds. A rough estimate of the parameters can be obtained from past experience or by some coarse method currently available in the literature, then the proposed method can be used to refine the solution and obtain more accurate results.

The results so far obtained deepen our understanding of generation of cell shape. One possibility of interpretation of the data is based on actin organization, the involvement of hydraulic pressure and cytoplasmic flow. The method is not limited to the appearance of interference fringes and thus allows a volume determination of any thin viscoelastic sample, as are e.g., sections of biological material or cells attached to a flat substratum.

APPENDIX

Reflection and transmission coefficients $R(m_1, m_2, \Theta)$ and $T(m_1, m_2, \Theta)$ of Eqs. 2, 3, 7, and 9 are given here.

If both mediums m_1 and m_2 have zero shear wave velocity, in other words, if m_1 and m_2 are not solid then

$$R(m_1, m_2, \Theta) = (\Gamma_2/\Gamma_1 - \delta_2/\delta_1)/(\Gamma_2/\Gamma_1 + \delta_2/\delta_1) \quad \text{(A1)}$$

$$T(m_1, m_2, \Theta) = 2/(\Gamma_2/\Gamma_1 + \delta_2/\delta_1), \quad \text{(A2)}$$

where

$$\delta_1 = (\Omega \cdot \cos \Theta)/\alpha_1$$

$$\delta_2 = [\Omega \cdot \cos \{\arcsin (\alpha_2 \cdot \sin \Theta/\alpha_1)\}]/\alpha_2. \quad \text{(A3)}$$

Ω, α_1, α_2, Γ_1, and Γ_2 are defined in the text. Eqs A.1 and A.2 are used when m_1 and m_2 stand for cell or coupling fluid.

If m_1 is a liquid and m_2 is a solid then $R(m_1, m_2, \Theta)$ takes the following form

$$R = (A - B)/(A + B), \quad \text{(A4)}$$

where

$$A = (\Gamma_2/\Gamma_1) \cdot [4k^2\delta_2\Phi_2 + (2k^2 - k_2^2)^2] \quad \text{(A5)}$$

$$B = (\delta_2/\delta_1) \cdot k_2^4 \quad \text{(A6)}$$

$$k = (\Omega \cdot \sin \Theta)/\alpha_1 \quad \text{(A7)}$$

$$k_2 = \Omega/\beta_2 \quad \text{(A8)}$$

$$\Phi_2 = [\Omega \cdot \cos \{\arcsin (\beta_2 \cdot \sin \Theta/\alpha_1)\}]/\beta_2. \quad \text{(A9)}$$

β_2 is the shear wave velocity in medium m_2. δ_1 and δ_2 are given in Eq. A.3. Eq. A.4 is used for computing $R(c, g, \Theta)$ of Eq. 9.

The authors would like to thank Mrs. C. Penzkofer for her technical help during the experiments.

Support of this research by an Alexander von Humboldt fellowship to Tribikram Kundu and by grants from the Deutsche Forschungsgemeinschaft (Be 423/13) is gratefully acknowledged.

Received for publication 9 July 1990 and in final form 17 January 1991.

REFERENCES

Bereiter-Hahn, J. 1987*a*. Scanning acoustic microscopy visualizes cytomechanical responses to cytochalasin D. *J. Microsc.* 146:29–39.

Bereiter-Hahn, J. 1987*b*. Comparison of the appearance of cells observed using scanning acoustomicroscopy with that obtained by interference and fluorescence microscopy. *Scanning Imaging Technol.* 809:162–165.

Bereiter-Hahn, J. 1987*c*. Mechanical principles of architecture of eukaryotic cell. *In* Cytomechanics. J. Bereiter-Hahn, O. R. Anderson, W. E. Reif, editors. Springer Verlag, Heidelberg, New York. 1–30.

Bereiter-Hahn, J., J. Litniewski, K. Hillmann, A. Krapohl, and L. Zylberberg. 1989. What can scanning acoustic microscopy tell about animal cells and tissues? *Acoust. Imaging.* 17:27–38.

Bereiter-Hahn J. 1988. Involvement of microcompartmentation in the regulation of cell proliferation. *In* Microcompartmentation. D. Jones, editor. CRC Press Inc., Boca Raton, FL. 55–69.

Bereiter-Hahn, J., C. H. Fox, and B. Thorell. 1979. Quantitative reflection contrast microscopy of living cells. *J. Cell Biol.* 82:767–779.

Bertoni, H. L., and T. Tamir. 1973. Unified theory of Rayleigh angle phenomena for acoustic beams at liquid-solid interfaces. *Appl. Physics.* 2:157–172.

Daft, C. M. W., J. M. Weaver, and G. A. Briggs. 1985. Phase contrast imaging of tissue in the scanning acoustic microscope. *J. Microsc.* 139: RP3–RP4.

Elson, E. L. 1988. Cellular mechanics as an indicator of cytoskeletal structure and function. *Annu. Rev. Biophys. Chem.* 17:397–430.

Hildebrand, J. A., D. Rugar, R. N. Johnston, and C. F. Quate. 1981. Acoustic microscopy of living cells. *Proc. Natl. Acad. Sci. USA.* 78:1656–1660.

Hildebrand, J. A., D. Rugar, and C. F. Quate. 1982. Biological acoustic microscopy—living cells at 37°C and fixed cells in cryogenic liquids. *Proc. Elect. Microsc. Soc. Am.* 40:174–177.

Hildebrand, J. A., and D. Rugar. 1984. Measurement of cellular elastic properties by acoustic microscopy. *J. Micros.* 134:245–260.

Izzard, C. S. 1976. Cell-to-substrate contacts in living fibroblasts: an interference reflexion study with an evaluation of the technique. *J. Cell Sci.* 21:129–159.

Johnston, R. N., A. Atalar, J. Heilserman, V. Jipson, and C. F. Quate. 1979. Acoustic microscopy: resolution of subcellular detail. *Proc. Natl. Acad. Sci. USA.* 76:3325–3329.

Karim, M. R., A. K. Mal, and Y. Bar-Cohen. 1990. Inversion of leaky lamb wave data by simplex algorithm. *J. Acoust. Soc. Am.* 88:482–491.

Kundu, T. 1990. A complete acoustic microscopical analysis of multilayered specimens. *ASME J. Appl. Mech.* In press.

Kushibiki, J., A. Ohkubo, and N. Chubachi. 1982*a*. Effect of leaky SAW parameters on $V(z)$ curves obtained by acoustic microscopy. *Electronics Lett.* 18:668–670.

Kushibiki, J., A. Ohkubo, and N. Chubachi. 1982*b*. Material characterization by acoustic line-focus beam. *Acoust. Imaging.* Plenum Press, New York. 12:101–111.

Kushibiki, J., Y. Matsumoto, and N. Chubachi. 1983. Material characterization by acoustic microscope with line-focus beam. *Acoust. Imaging.* Plenum Press, New York. 13:193–202.

Levesque, M. J., E. A. Sprague, C. J. Schwartz, and R. M. Nerem. 1989. The influence of shear stress on cultured vascular endothelial cells: the stress response of an anchorage-dependent mammalian cell. *Biotechnol. Progr. 5:1–8.*

Liang, K., B. T. Khuri-yakub, S. D. Bennett, and G. S. Kino. 1983. Phase measurements in acoustic microscopy. *Proc. Ultrasonics Symp. Atlanta USA.* 2:591–604.

Litniewski, J., and J. Bereiter-Hahn. 1990. Measurements of cells in culture by scanning acoustic microscopy. *J. Microsc.* 158:95–107.

Nelder, J. A., and R. Mead. 1965. A simplex method for function minimization. *Comput. J.* 7:308–315.

Parmon, W., and H. L. Bertoni. 1979. Ray interpretation of the material signature in the acoustic microscope. *Electron Lett.* 15:684–686.

Quate, C. F. 1980. Microwaves, acoustics, and scanning microscopy. *In* Scanned Imaging and Microscopy. E. A. Ash, editor. Academic Press, London. 23–55.

Schmid-Schönbein, G. W., K. L. P. Sung, H. Tozeren, R. Skalak, and S. Chien. 1981. Passive mechanical properties of human leukocytes. *Biophys. J.* 36:243–256.

Somech, M. G., G. A. D. Briggs, and C. Ilett. 1983. Detection of surface-breaking cracks in the acoustic microscope. *Acoust. Imaging.* Plenum Press, New York. 13:119–128.

Waugh and Hochmuth. 1987. Cytomechanics. J. Bereiter-Hahn, O. R. Anderson, and W. E. Reif, editors. Springer Verlag, Heidelberg, New York. 249–260.

Weglein, R. D. 1979. A model for predicting acoustic material signature. *Appl. Phys. Lett.* 34:179–181.

Weglein, R. D. 1980. Acoustic microscopy applied to SAW dispersion and film thickness measurement. *IEEE (Inst. Electr. Electron. Eng.) Trans. Sonics Ultrason.* SU-27:82–86.

Weglein, R. D. 1982. Non-destructive film thickness measurement on industrial diamond. *Electr. Lett.* 18:1003–1004.

Worthen, G. S., B. Schwab III, E. L. Elson, and G. P. Downey. 1989. Mechanics of stimulated neutrophils: cell stiffening induces retention in capillaries. *Science (Wash. DC.).* 245:183–186.

Yamanaka, K., Y. Enomoto, and Y. Tsuya. 1982. Application of scanning acoustic microscopy to the study of fracture and wear. *Acoust. Imaging.* Plenum Press, New York. 12:79–87.